



## Structural, morphological, magnetic and adsorption properties of Fe<sub>3</sub>O<sub>4</sub> for copper removal from aqueous solution

Syazana Sulaiman<sup>a,\*</sup>, Raba'ah Syahidah Azis<sup>a,b,\*</sup>, Ismayadi Ismail<sup>a</sup>, Abdul Halim Shaari<sup>b</sup>, Haslina Che Man<sup>c</sup>, Nur Asyikin Ahmad Nazri<sup>a</sup>, Ayuni Azuan<sup>b</sup>

<sup>a</sup>Material Synthesis and Characterization Laboratory (MSCL), Institute of Advanced Technology (ITMA), Universiti Putra Malaysia, 43400 UPM Serdang, Selangor, Malaysia, Tel. +603-9769 6666; emails: syazana2104@gmail.com (S. Sulaiman), rabaah@upm.edu.my (R.S. Azis), ismayadi@upm.edu.my (I. Ismail), asyikin2750@uitm.edu.my (N.A. Ahmad Nazri)

<sup>b</sup>Department of Physics, Faculty of Science, Universiti Putra Malaysia, 43400 UPM Serdang, Selangor, Malaysia, emails: ahalim@upm.edu.my (A.H. Shaari), ayuniazuan@yahoo.com (A. Azuan)

<sup>c</sup>Department of Biological and Agricultural Engineering, Faculty of Engineering, Universiti Putra Malaysia, 43400 UPM Serdang, Selangor, Malaysia, email: hasfalina@upm.edu.my

Received 8 October 2019; Accepted 17 October 2020

---

### ABSTRACT

In this work, the magnetite nanoparticles (MNP) were synthesized from steel waste product and used as an adsorbent to remove metal copper (Cu) in an aqueous solution. The magnetite powders were mechanically alloying using high energy ball milling for 3, 6, and 9 h to produce MNP. The structural, composition, magnetic properties and morphological of the MNP were characterized using X-ray diffraction and Fourier-transform infrared spectroscopy, vibrating sample magnetometer and transmission electron microscopy, respectively. The adsorption parameters and the surface area of the MNP were studied using a Brunauer–Emmett–Teller and atomic absorption spectrophotometer. The parameters of contact time, temperature, pH, adsorbent dosage, and initial Cu concentration of the solution were investigated. The kinetic studies of the pseudo-second-order model were successfully employed. Langmuir model ( $R^2 > 0.993$ ) were more correspond with the adsorption isotherm data of Cu(II) ions. According to the results from adsorption thermodynamic studies, it can be inferred that the main adsorption mechanism between MNP adsorbent and Cu(II) ions is ion-exchange–surface mechanism. The highlight of this work is the adsorption properties and the characterization of the MNP as a natural, low-cost and good potential adsorbent for the waste treatment process.

*Keywords:* Magnetite nanoparticles (MNP); Steel waste product; Adsorbent; Adsorption; Isotherm; Cu

---

### 1. Introduction

Clean water is important for our everyday life. It is crucial for humans to get clean water on daily basis activities such as drinking, cleaning, industry, farming, and agriculture. However, with the rapid growth of industrial

development, the pollution of water has risen a big issue in obtaining clean water. The wastes produced by the chemical from the industrial process were dumped into the river, lake, and ocean which contribute to the production of wastewater. Wastewater is a combination of liquid or water-carried wastes that consist of impurities and pollutant

---

\* Corresponding authors.

substances in the form of solids or gasses. The wastewater contains chemical substances and heavy metal pollutants. Recently, heavy metal pollution that has excessively released into the environment and become one of the major global concern to the environment due to rapid industrialization and urbanization [1]. There are enormous heavy metals in industrial wastewater, such as cadmium, zinc, lead, chromium, nickel, copper, platinum, arsenic, and mercury. Heavy metals are highly toxic to human health and aquatic organism. Besides, heavy metals affect the yield, growth, and quality of crops. These toxic metals that are exposed to humans and the environment pose several serious health problems and environmental hazards [2].

The environmental problem causes severe health because they are persistent in nature, non-biodegradable to the environment [3]. Even though the metals are needed in small quantities for health, but the high level of metals like copper may be toxic in the present study. Copper (Cu) is categorized to be one of the most toxic heavy metals and has significant effects on living organisms. Cu ion is a heavy cation found commonly in industrial wastewater [4]. Besides, high doses of Cu can cause anemia, intestinal irritation, liver, kidney damage, intravascular hemolysis, hematuria, and gastrointestinal bleeding [5]. Due to the toxicity, non-degradability, easy accumulation of elements, the removal of Cu from wastewater has attracted much interest worldwide [6].

Recently, great attention has been a concern by researchers and scientists to eliminate harmful pollutants from both air and water using a natural product and widely available in sorption treatment [7]. Besides, numerous approaches have been studied for low-cost, more effective technologies developed to improve the quality of water. Over the past decades, the researchers have carried out low-cost and high capacity adsorbents for water remediation. In this regard, the adsorption method is a simple, attractive, universal, and efficient treatment to remove contaminants within the aqueous phase [8]. Besides, adsorption is one of the effective treatments that can replace high-cost wastewater treatment methods because of its simplicity, convenience, and high removal efficiency [9].

Magnetic separation has widely used because of the fast, efficient, cost-effective method in water treatment technology [10–13]. The application of magnetite nanoparticles (MNP) is more attractive for the removal of heavy metals contamination from the wastewater because of their essential features like small particle size, high surface area, and has a magnetic property. MNP is promising for industrial-scale wastewater treatment due to its low cost, strong adsorption capacity, easy separation, and enhanced stability [14]. In this paper, we intend to highlight the adsorption of Cu metal using MNP in aqueous solutions.

Besides, the nanoparticles are widely studied for their feasibility as a filter, and a fantastic result was highlighted [15]. Despite their advantages in removing several metals, the present work aimed to study the effectiveness of MNP for different particles size that milled at different milling hours were investigated. The preparation and surface characterization of the adsorbent were discussed critically. The isotherm adsorption models and kinetic studies were studied in detail.

## 2. Experimental

### 2.1. Preparation of adsorbents

Firstly, the iron oxides were extracted from the mill scale waste product. The mill scales were weighted for about 100 g and then milled using conventional milling for 24 h to obtain the desired size. The resultant mill scales waste powder was subjected to the magnetic separation technique and curie temperature separation technique [10,13]. The magnetic material was dried in an oven for 24 h at 80°C. The magnetite powder was undergoing mechanical alloying (MA) by conventional before subjected to high energy ball milling (HEBM) for 3, 6, and 9 h to produce the nano-sized particles.

### 2.2. Adsorbents MNP characterization

Phase formation of the powder and the sintered samples were characterized using X-ray diffraction (XRD) in a Philips X'Pert PRO X-ray (Model PW3040) diffractometer with Cu K $\alpha$  radiation with graphite monochromator using Cu-K $\alpha$  radiation with  $\lambda = 1.54 \text{ \AA}$  using 2 $\theta$  scan mode from 20° to 80° and a 0.03° scan step at room temperature. The database of the JCPDS data was used for the interpretation of XRD spectra. The structural characterization of the samples was carried out using the PANalytical Highscore Plus Software. The magnetization M-magnetic field H (M-H) hysteresis curves of the MNP were measured using a vibrating sample magnetometer LAKESHORE Model 7404 at room temperature under an applied magnetic field from 0–13 kG (0–1.3 T).

The BELSORP-mini II Brunauer–Emmett–Teller (BET) machine was used to measure the specific surface area and pore size of the samples. The N<sub>2</sub> adsorption–desorption at the liquid nitrogen temperature using a NOVA 2200e automatic surface area and porosity analyzer. About 0.2 mg of samples were degassed at 120°C for 8 h under 1 Pa vacuum condition before measurement to remove the humidity in the samples. Nitrogen gas was purged with 10–100 mL/min of the gas flow into the sample cell, and the samples were put into a Dewar vessel containing 2 L of nitrogen liquid, and the measurement of surface area per mass was determined.

The resultant of MNP milled particles were examined using a JEOL JEM-2100F field-emission transmission electron microscopy (TEM) for nanometer-size confirmation. For TEM sample preparation, the MNP powder particles were dispersed in an acetone solution and leave the samples under UV light. The samples were then dispersed in the ultrasonic sonicator for several hours. The morphology of the MNP was then determined under the observation of TEM. The distribution of the particle size was obtained by calculating the average diameter of at least 100 different particle images by using J-Image software.

### 2.3. Batch adsorption and kinetic studies

The reagents used for synthesis 0.01 M (2416 mg/L) of copper stock solutions were prepared by dissolving 1 L distilled water and copper nitrate in a volumetric flask. 1.0 g of MNP was added to 15 mL of copper solution in the beaker. The solution was stir for several minutes before being separated by the external magnetic field. Batch adsorption

of copper ions onto MNP adsorbents was conducted under four different conditions. The effect of contact time, adsorbent dosage, pH, and temperature on the adsorption of Cu by MNP from aqueous solutions were investigated. All batch adsorption was investigated in an aqueous solution for an initial Cu ion concentration of 0.01 M.

Firstly, the effect of contact time was examined to find the suitable contact time at which the nanoparticles are saturated, and the adsorption is at equilibrium. The contact time used was 5, 10, 15, 20, 25, and 30 min. The copper stock solutions were treated with 1.0 g of MNP at room temperature at different periods of contact times. After adsorption reached equilibrium, the adsorbent was conveniently separated via an external magnetic field. Secondly, the effect of adsorbent dosage was examined by varying the amount of adsorbent from 0.2–1.0 g. Thirdly, the effect of pH solution was investigated with ranging from pH 1 to pH 5 using a pH meter by adding  $H_2SO_4$ . Then, the effect of temperature on Cu(II) adsorption experiment was determined by varied the temperature of 30°C, 40°C, 50°C, 60°C, 70°C, and 80°C at pH 5 and treated with 1.0 g of MNP. The adsorption capacities of the Cu concentrations were determined using atomic absorption spectroscopy (AAS) (Thermo Scientific iCE 3000 Series Solaar AA).

The initial and final concentrations of the sample solutions were measured by AAS. For kinetic studies, experiments were conducted with 15 mL copper nitrate solutions of concentration 2,416 mg/L, maintained at pH 5, room temperature at a different contact time of 0–30 min of 1 g of MNP. The amount of Cu ion adsorbate was taken up by an MNP adsorbent as a function of the concentration of adsorbate at a constant temperature was called the adsorption capacity ( $q_e$ ), and percentage removal, RE (%) was determined as in Eqs. (1) and (2) [16,17]:

$$\%RE = \frac{C_0 - C_e}{C_0} \times 100 \quad (1)$$

$$q_e = \frac{V}{m}(C_0 - C_e) \quad (2)$$

where  $q_e$  (mg/g) is the amount of adsorbate per unit mass of adsorbent at time  $t$ .  $C_0$  and  $C_e$  are the initial and final concentrations (mg/L) of the solution, respectively.  $V$  is the volume of the solution in L, and  $m$  is the mass of the adsorbent in g. All experiments were repeated two times, and average values were reported.

Table 1

Highest peak position,  $hkl$ , full width at half maximum,  $d$ -spacing, crystal structure, chemical formula, ICSD, and space group of samples

Sample	Highest pos. ( $^{\circ}2\theta$ )	$hkl$	Height (cts.)	FWHM ( $^{\circ}2\theta$ )	$d$ -spacing (Å)	Crystal structure	Chemical formula	ICSD	Space group
3 h	35.764	113	437.57	1.5759	2.50865	Cubic	$Fe_3O_4$	98-010-9828	Fd-3 m
6 h	35.5266	113	363.13	1.7718	2.52486	Cubic	$Fe_3O_4$	98-010-9823	Fd-3 m
9 h	35.6967	113	423.36	2.5600	2.53322	Cubic	$Fe_3O_4$	98-010-9827	Fd-3 m

### 3. Results and discussion

#### 3.1. Structural analysis of MNP nanoparticles

Fig. 1 shows the XRD spectra of magnetite powder milled at different milling times, 3, 6, and 9 h. The diffraction spectra of the materials revealed the presence of magnetite, MNP for all milling time. The diffraction angle at  $2\theta$  of 30.272, 35.659, 37.334, 43.3543, 57.2950, 62.9057, and 74.4039 which can be indexed to (022), (113), (222), (004), (133), (224), (115), (004) confirms the signature peaks of a cubic unit cell  $Fe_3O_4$ , respectively. The XRD spectra were matched to the ICSD of magnetite with a space group of Fd-3m and lattice parameter ( $a = b = c$ ) of 8.3440 Å. The XRD parameter of the highest intensity  $2\theta$  is tabulated in Table 1. With increase milling time, the magnetite powder achieves high purity magnetite samples. It shows that as milling time increases, the formation of nanocrystalline magnetite is determined by the broadening of XRD peaks. The average particle size was estimated by using the Debye–Scherrer formula (Scherrer 1918) in Eq. (3):

$$D = \frac{0.9\lambda}{\beta \cos\theta} \quad (3)$$

where  $D$  is particle diameter size,  $\lambda = 0.1541$  nm,  $\beta$  is the full width at half maximum (FWHM), and  $\theta$  is the diffraction

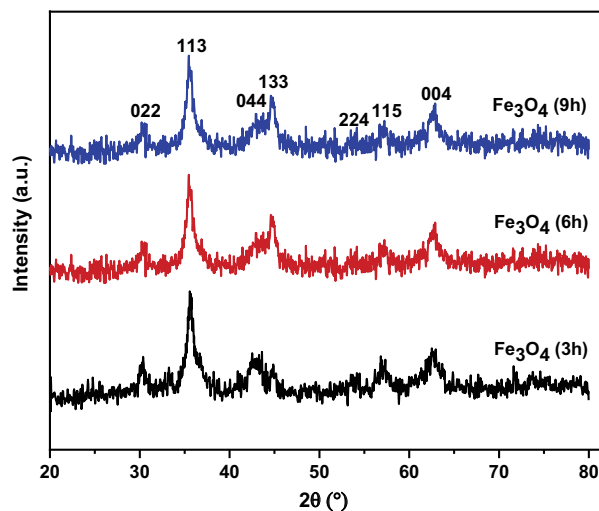


Fig. 1. X-ray diffraction spectra of crystallite magnetite nanoparticles milled for 3, 6 and 9 h.

angle. The effect of the crystallite size of MNP with milling time is shown in Fig. 2.

The crystallite sizes obtained show a decreasing trend of 5.5 and 4.9 nm for 3 and 6 h milling time, respectively. By increasing the milling time to 9 h, the particle size was slightly increased by 9.6 nm. During the milling process, the powder was collided with the steel balls and milled in the vial. The energy of the collision between the balls and vial is transferred to the powders and heating the powder continuously. By prolong milling the time, more heat is transferred to powder. Continuous collisions in the milling process give heat generation during the milling process. Hence, the particle size was increased as an increase in the milling hour. The nanometer scaled diffusion are produced during high energy mechanical milling. This involves cold-welding and fracture of milled powders. Thus, atomic diffusivity is improved through the formation of a large number of structural defects. As a result, metastable phases form at the early stage of the milling process. The line broadening of MNP for 9 h milled was shaper compared to MNP milled for 3 and 6 h. This effect can be explained by the increase of particle size, and the crystallinity was improved [18]. The Bragg peaks intensities decrease with increasing milling time, and considerable line broadening can also be observed. As an increase in the milling time, the amount of defect also increased [19].

TEM images are shown in Fig. 3 and displayed the diameter measured for 100 particles. The micrographs show sphere-morphological shape particles which favor the ceramic processing technique [20]. The TEM micrographs show on each of the nanoparticles is agglomerated, even though a sonication process was done before the TEM measurement. These agglomerations might be due to the large surface area and the magnetic forces of the MNP nanoparticles after subjected to HEBM. The alloying and cold welding between the particles during the milling process also contributes to these agglomerations. However, this is a natural consequence of the MA technique products due to

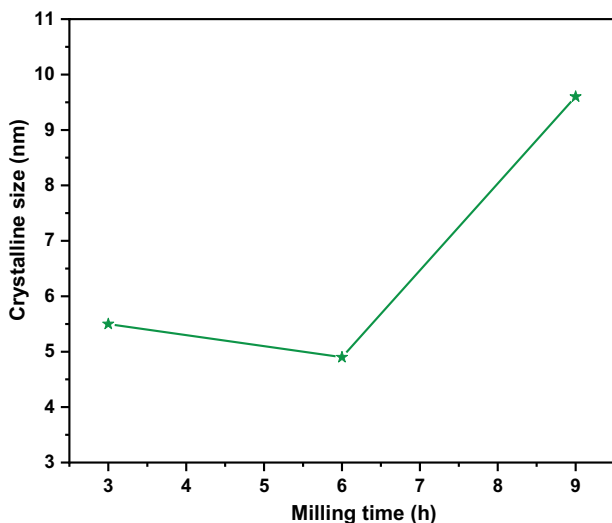


Fig. 2. Crystallite sizes vs. milling time (h) for magnetite nanoparticles after high energy ball milling.

the high impact velocity of the milling media to the particles [21]. To reduce the agglomeration that occurred on the nanoparticle, the surface coating on the nano-adsorbent surfactant needs to be conducted [22]. The particle size distributions of MNP nanoparticles are shown in histograms in Fig. 3 and Table 2. After 6 h of milling, nano-sized particles in the range of 6–11 nm on average were obtained. In Fig. 4 are shown field-emission scanning electron microscopy and energy-dispersive X-ray diffraction analyses revealed the presence of Fe and O in a high percentage of 53.74%.

### 3.2. Magnetic hysteresis analysis of MNP

Fig. 5 shows an overlapping hysteresis curve of MNP powder. The curves indicate a superparamagnetic-ferromagnetic behavior for all the studied samples, as evidenced by zero remanences on the magnetization loop. The measured values of saturation magnetization ( $M_s$ ) are presented in Table 3. The  $M_s$  value decreases with the increase in the milling time. The  $M_s$  value is higher at lower milling time, 3 h. The estimated sizes of particles, as determined from TEM images, and saturation magnetization, are linearly correlated (Figs. 3, 5, Tables 2 and 3). This means that the first direct effect of reducing particle sizes of samples is lowering the corresponding saturation magnetization values. On average, the bigger the particle is, the higher the saturation magnetization of the MNP. MNP amorphization decreased their crystallinity due to the poor super-exchange interaction between magnetic moment per unit mass sample [21].

### 3.3. BET analysis

Fig. 6a shows the  $N_2$  adsorption and desorption isotherm curve of MNP. Nitrogen adsorption using BET was used to characterize the porous and surface area property of MNP. Morphological features such as surface area per volume, pore-volume, pore size, and type of adsorbent were obtained from isotherm adsorbents are presented in Table 4. The nitrogen adsorption-desorption isotherms were determined over the range of relative pressure. Fig. 6a proved type III, which indicates the characteristic of mesoporous material (pore size between 20–500 Å) [23]. Mesopores offer more available sites for adsorption and plays an important role as a transportation channel that allows adsorbate molecules to diffuse from bulk into adsorbent [24]. Indeed, it has been proved that MNP were porous that metal ion could diffuse in these pores, increasing percentage removal [25].

Fig. 7 shows the spectrum  $Fe_3O_4$  before and after adsorption of Cu(II) ions. The Fourier-transform infrared spectra reveal a strong characterization peak at  $3,478\text{ cm}^{-1}$  that corresponds to O–H due to inter and intramolecular hydrogen bonding at polymeric compound [26]. The peak at  $2,835\text{ cm}^{-1}$  is attributed to the C–H vibration and shows the free hydroxyl group on the adsorbent surface. This may result from the high electron density induced by the adsorption of Cu(II) ion onto  $Fe_3O_4$ . The adsorption bands at  $525\text{ cm}^{-1}$  ( $nFe_3O_4$ ) shifted to  $576\text{ cm}^{-1}$  ( $Cu:nFe_3O_4$ ) due to the Fe–O band that adsorbed Cu(II) ion from aqueous medium [27]. Besides, there is an obvious absorption band at a low frequency in the range  $400\text{--}700\text{ cm}^{-1}$ , which indicates the

TEM image with average particles sizes

Particles size distribution of MNP

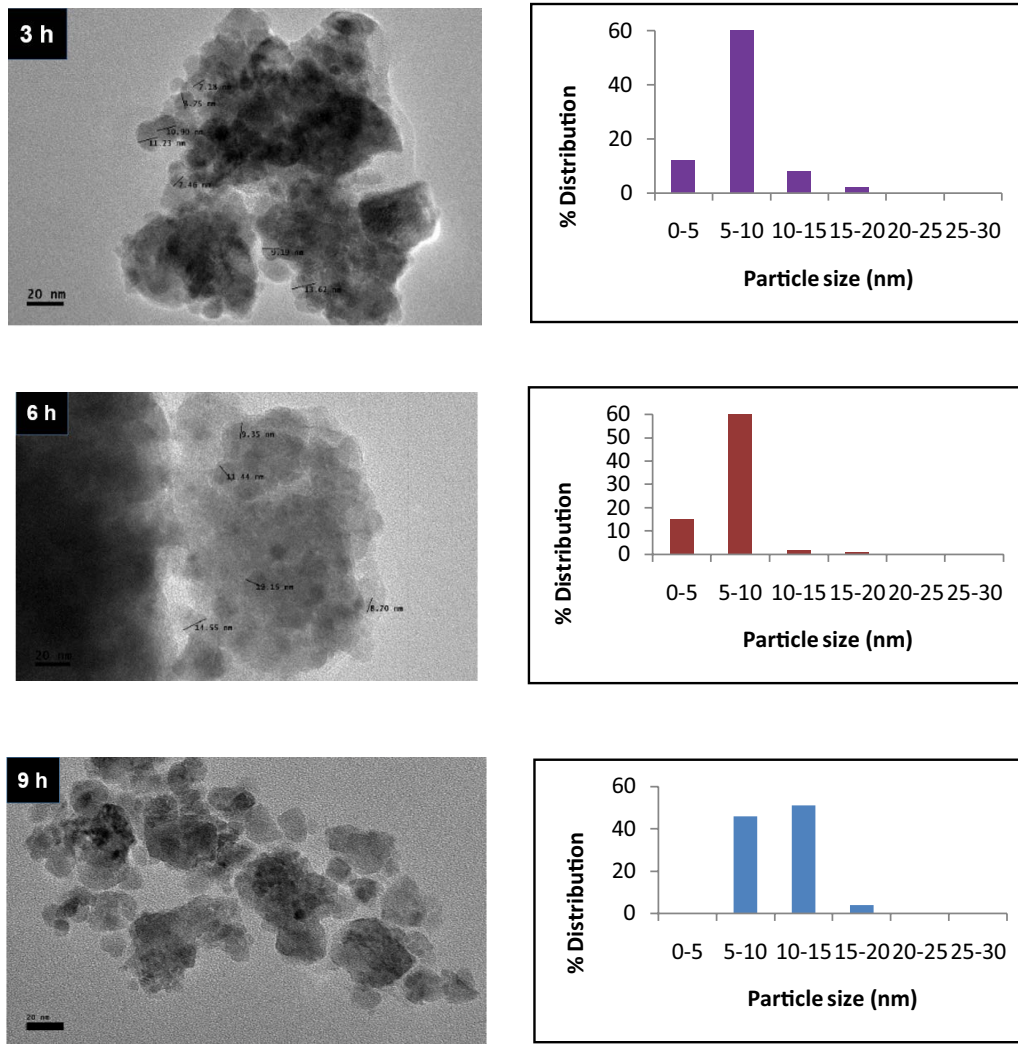


Fig. 3. Transmission electron microscopy micrograph at 20 nm scale bar at 3, 6 and 9 h.

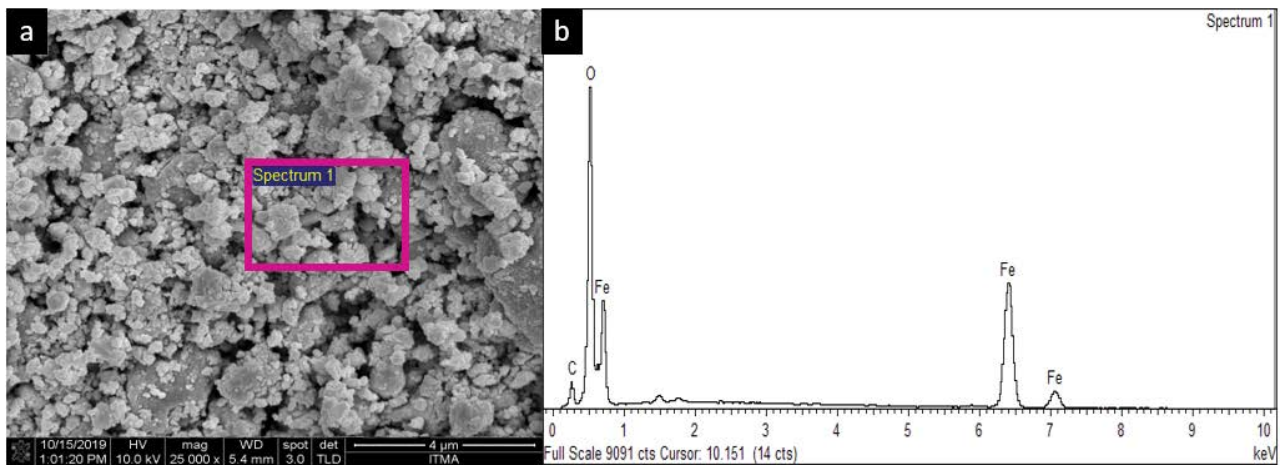


Fig. 4. (a) Field-emission scanning electron microscopy milled for 7 h and (b) energy-dispersive X-ray diffraction analysis of  $Fe_3O_4$ .

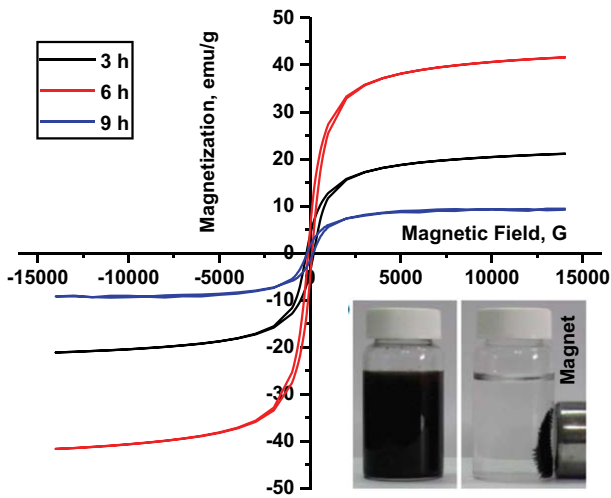


Fig. 5. Overlapping hysteresis loops of magnetite nanoparticles (a) 3, (b) 6 and (c) 9 h.

Table 2

Particle size and crystallite size of magnetite nanoparticles by transmission electron microscopy and XRD

Milling time (h)	Transmission electron microscopy particles size, $d_{\text{TEM}}$ (nm)	Crystallite size, $d_{\text{XRD}}$ (nm)
3	7.42	5.5
6	6.29	4.9
9	10.35	9.6

stretching vibration of the Fe–O bond. The peak of Fe–O has a slight shift from 525 to 576  $\text{cm}^{-1}$  as Cu(II) ion has to get adsorbed onto the  $\text{Fe}_3\text{O}_4$  [28]. The changes in pH value are strongly influenced by the characteristics of the  $\text{Fe}_3\text{O}_4$  [29]. Thus, three functional groups that shift are likely involved in Cu binding [30].

### 3.4. Mechanism of the Cu(II) ion on MNP

Fig. 8 presents the mechanism on the MNP of the Cu(II) ion adsorption. It suggests the exchange of ion process as an adsorption principle for the removal of copper. This contains a phenolic compound that has an active site for the mechanism of adsorption. Cu(II) ion was attached to two adjacent hydroxyl groups and two oxyl-groups that could donate two pairs of electrons to the metal ion and forming four coordination and two hydrogen ions ( $\text{H}^+$ ) into solution [31]. Fig. 8 demonstrates the pseudo-second-order model that fit for Cu(II) adsorption suggesting that the rate-controlling mechanism of chemisorption was mainly involved. Similar trends have been detailed in previous literature [32].

### 3.5. Effect of environmental parameters

The surface characteristics of the adsorbent surface are controlled by the contact time, adsorbent dosage, pH, temperature [33]. Therefore, batch adsorption was carried out to study these environmental parameters.

#### 3.5.1. Effect of contact time

Fig. 9a illustrates the effect of contact time on the adsorption capacity and rate of Cu(II) uptake onto MNP. The effect of contact time was evaluated to identify the efficiency of MNP for the removal of Cu(II). The Cu(II) was rapidly removed within 5 mins of the experiment. The results show that after 5 min MNP added in Cu aqueous solution, the concentration of metals was at equilibrium ( $C_e$ ), at which the amount of metal desorbed is equal to the amount of metal adsorbed. From the observation, the adsorption process for MNP almost finished within 30 min, whereas, a faster process was observed at 90 min MNP previously reported by [5]. The faster adsorption rate by the MNP could be attributed to the ion exchange-surface mechanism [34] and the monolayer surface adsorption by a non-porous MNP adsorbent [35].

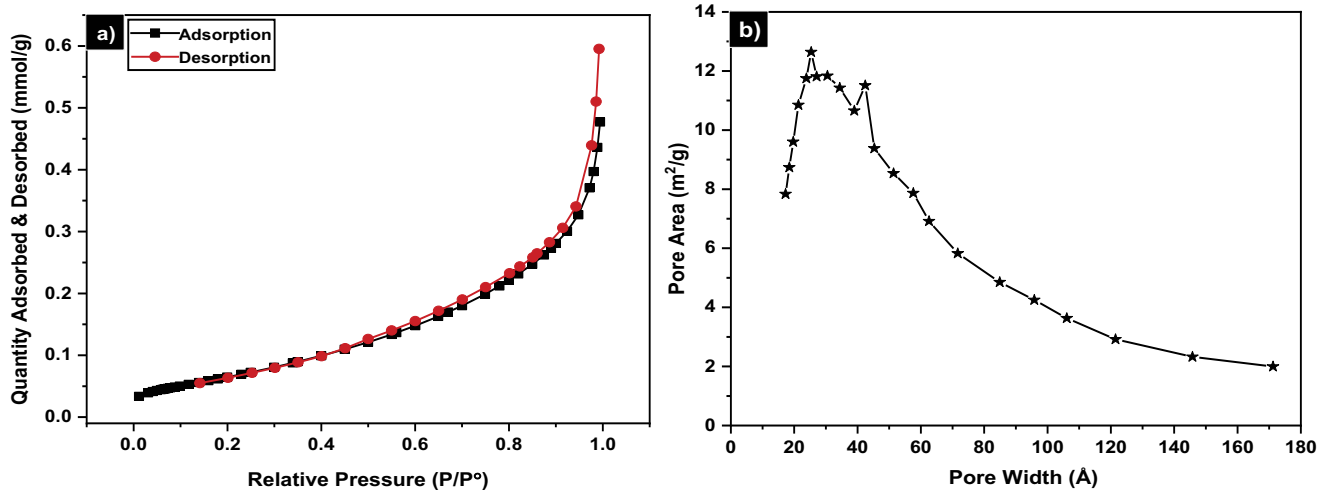


Fig. 6. a)  $\text{N}_2$  adsorption and desorption isotherm curve and (b) distribution of the pore size of magnetite nanoparticles.

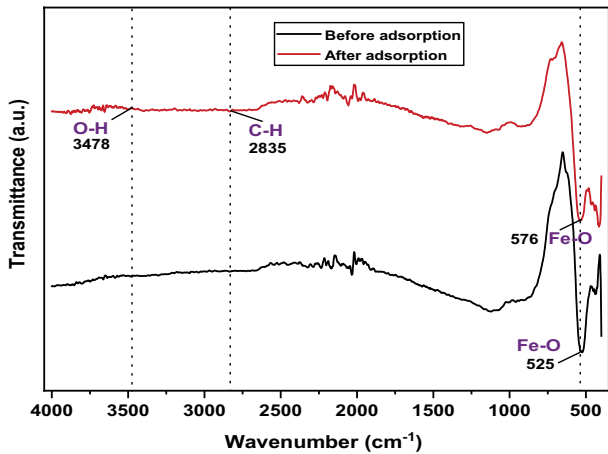


Fig. 7. Fourier-transform infrared spectra of  $\text{Fe}_3\text{O}_4$  before and after adsorption of  $\text{Cu(II)}$  ion.

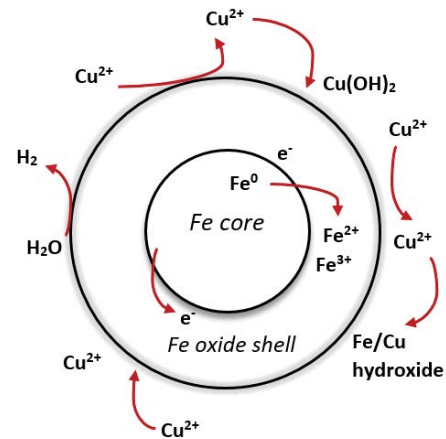


Fig. 8. Schematic diagram of mechanism adsorption of  $\text{Cu(II)}$  and magnetite nanoparticles.

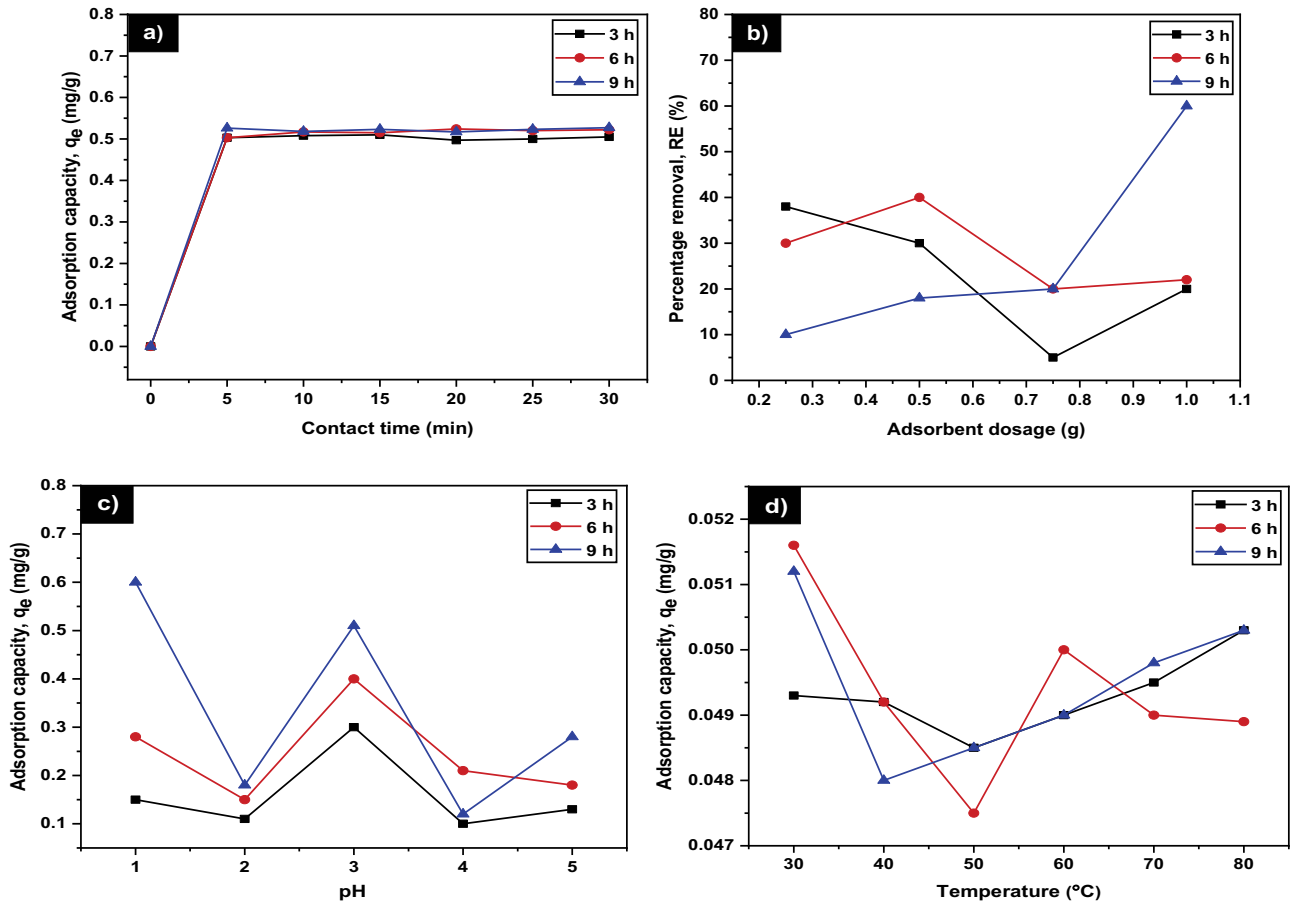


Fig. 9. The adsorption capacity of  $\text{Cu(II)}$  on magnetite nanoparticles at (a) contact time, (b) adsorbent dosage, (c) pH, and (d) temperature.

The initial concentrations which in turn may have provided the higher driving force for the ions from the solution to the adsorbents. The result may be more collisions between  $\text{Cu}$  ions and active sites on the MNP [36]. Since nearly all the adsorption sites of MNP existed on their exterior, it

was easy for the adsorbate to access these active sites, thus resulting in a rapid approach to equilibrium. This result is promising under the economic viability as equilibrium time plays a major role in designing a wastewater treatment plant. Similar observations and results were reported [6].

### 3.5.2. Effect of MNP dosage

Fig. 9b shows the percentage removal of Cu(II) with respect to the dosage of MNP. The adsorbent dosage is an essential parameter in adsorption studies because it determines the capacity of the adsorbent for a given concentration of the metal ion solution. The results show the MNP milled for 9 h shows the higher adsorption Cu(II) capacity percentage as the MNP dosage increases. This due to the increases in a certain area and the probability of collision between particles of adsorbent and metal ions [37]. However, the percentage removal of copper by MNP milled for 3 and 6 h shows a decreasing trend as the number of dosage increases. This may be due to the adsorption of almost Cu(II) ions to the adsorbent and the establishment of equilibrium between Cu(II) molecules adsorbent to the adsorbent and those remaining unadsorbed in the solution.

### 3.5.3. Effect of pH

The removal of Cu(II) from aqueous solution through adsorption is highly dependent on the initial solution pH that determines the surface charge of the adsorbent and the adsorbate speciation. The effect of pH on the adsorption of Cu(II) onto MNP is shown in Fig. 9c. It is observed that the pH is increased from 1.0 to 3.0, the percentage removal of copper will also increase before the percentage removal drops at pH 4.0 to 5.0. The adsorption capacity of Cu(II) ion with the solution pH due to less insignificant competitive adsorption of hydrogen ions [38]. There is an electrostatic interaction between the adsorbent and the metal adsorbents [39]. The results show that the optimum pH of the experimental system is pH to prevent Cu(II) from precipitation. The pH increased from 0.15 to 0.6 mg/L, the increment of pH from 1.0 to 5.0, indicating that the adsorption capacity of Cu(II) to MNP was highly pH-dependent.

### 3.5.4. Effect of temperature

Fig. 9d shows the thermodynamics experiment by heating the solution with MNP in the temperature range from 30°C to 80°C. The pH of the solution was pH 5, and 1.0 g of MNP milled at different milling time was used as an adsorbent. The adsorption capacity was increased at higher temperatures, which for MNP powder milled at 9 h, the percentage removal increased from 5.20% to 5.52% with increment temperature 30°C–80°C. The same trend was also observed for 6 and 3 h samples. This suggesting that adsorption of Cu(II) on to MNP is an endothermic process [40].

### 3.6. Adsorption kinetics

Kinetic studies are essential in an adsorption process that determines the uptake rate performance of the MNP adsorbate. The kinetic studies control the residual time for the entire adsorption process. The adsorption kinetics of Cu(II) on MNP was determined using similar procedures to those used in the batch adsorption studies. Lagergren's pseudo-second-order kinetic models were selected in this study to describe the adsorption process. The adsorption data were stimulated by the pseudo-second-order model, which is expressed by the following equation [41–43]:

$$\frac{t}{q_e} = \frac{1}{k_2 q_e^2} + \frac{t}{q_e} \quad (4)$$

where  $k_2$  is the rate constant of the second-order adsorption (g/mg h). The values of  $q_e$  and  $k_2$  were determined from the slope and the intercept of the plot of  $t/q_t$  vs.  $t$  (Fig. 10) are shown in Table 3. The calculated  $q_e$  values are in agreement with the theoretical values and the graph shows good linearity with  $R^2$  above 0.99. Therefore, the adsorption kinetics follows the pseudo-second-order model. The adsorption kinetic is represented by the pseudo-second-order model, involving donation or electron exchange between adsorbate and adsorbent [22].

### 3.7. Adsorption isotherms

Langmuir isotherm model is maximum adsorption that corresponds to a monolayer coverage of adsorption surfaces and predicted that metal ion adsorption takes place on the homogenous surface of the materials [13]. The linear form of the Langmuir adsorption isotherm model and its separation factor  $R_L$  as in Eq. (5) [44,45]:

$$\frac{C_e}{q_e} = \frac{1}{q_m K_L} + \frac{C_e}{q_{\max}} \quad (5)$$

where  $q_e$  (mg/g) is the amount adsorbed at equilibrium,  $C_e$  (mg/L) is the adsorbate concentration at equilibrium,

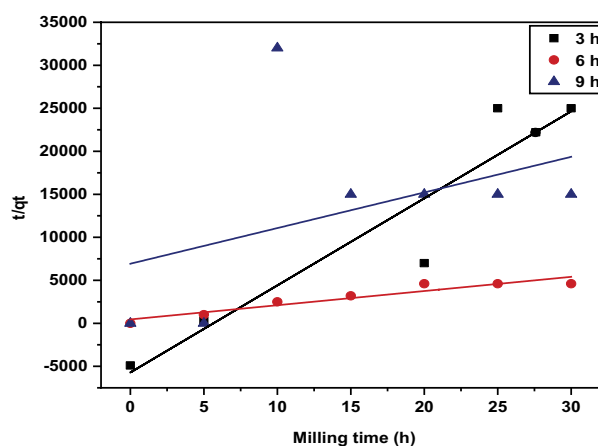


Fig. 10. Pseudo-second-order kinetics models for the adsorption of Cu(II) for 3, 6 and 9 h.

Table 3  
Magnetic parameter of magnetite nanoparticles at 3, 6 and 9 h

Milling time (h)	Magnetization saturation (emu/g)	Coercivity (G)
3	76.56	202.96
6	11.66	232.81
9	10.26	89.37

Table 4  
Morphological characteristics of magnetite nanoparticles obtained by N<sub>2</sub> adsorption

Milling hour (h)	Surface area per volume (m <sup>2</sup> /g)	Pore size (Å)	Pore volume (cm <sup>3</sup> /g)	Type of adsorbent
3	4.9236	77.0499	0.009484	Mesoporous
6	5.9970	67.9336	0.010185	Mesoporous
9	6.8254	72.3339	0.012343	Mesoporous

Table 5  
Kinetic parameter of pseudo-second-order kinetic model for the adsorption of Cu(II) ion

Adsorbent (h)	$q_e$ (mg/g) (calculated)	$C_i$ (mg/L)	Pseudo-second-order		
			$q_e$ (mg/g) (experimental)	$k_2$ (g/mg/min)	$R^2$
3	0.001	2,416	0.333	−2.383	0.8868
6	0.004	2,416	1.005	300.00	0.9104
9	0.001	2,416	1.051	34.394	0.1681

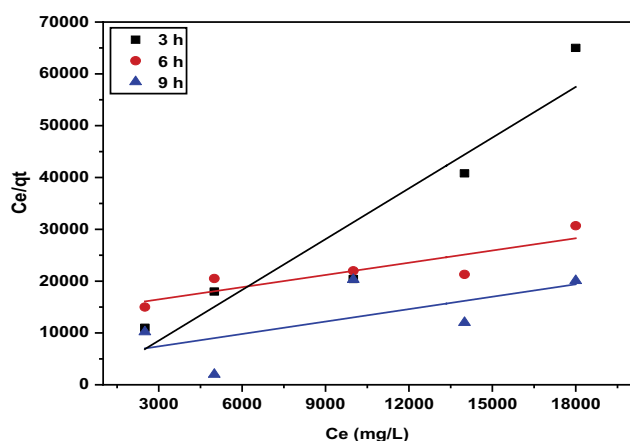


Fig. 11. Langmuir isotherm model for the adsorption of Cu(II) ion.

$q_{\max}$  (mg/g) represent the maximum amount adsorbed in monolayer,  $K_L$  in the Langmuir adsorption constant,  $b$  (L/mg) is the Langmuir constant related to adsorption energy. Langmuir constant  $q_{\max}$  and  $b$  were calculated from the slope and intercept of the linear plot of  $C_e/q_e$  vs.  $C_e$  (Table 4). The maximum Langmuir adsorption capacity was found 0.0039 mg/g. The Langmuir separation factor ( $R_L$ ) which is dimensionless constant, indicates whether the adsorption process is favorable or not [46].

#### 4. Conclusion

This study focused on the adsorption efficiency of MNP adsorbent from an aqueous solution for a toxic copper metal ion. The characterization studies revealed the various physicochemical properties of MNP, which are favorable for metal removal. Comparative preliminary batch studies demonstrated not only the optimal process parameters for maximizing metal sorption but also the principle underlying mechanism. Langmuir adsorption

Table 6  
Langmuir model correlation coefficients and constants for adsorption of Cu(II) ion

Isotherm model	Milling time (h)	Parameters	Values
Langmuir model	3	$q_{\max}$ (mg/g)	0.333
		$b$ (L/mg)	0.000
		$R^2$	0.888
Langmuir model	6	$q_{\max}$ (mg/g)	1.005
		$b$ (L/mg)	0.00008
		$R^2$	0.7824
Langmuir model	9	$q_{\max}$ (mg/g)	1.052
		$b$ (L/mg)	0.0001
		$R^2$	0.440

plot showed maximum Cu removal by MNP at 0.0039 mg/g at optimal conditions, and kinetic studies revealed the feasibility of the process. The pseudo-second-order model is determined as the best fit model at  $R^2 = 0.9104$ . The desorption studies indicate a fulfilling of essential criteria for advanced adsorbents. The developed MNP has demonstrated a superparamagnetic compound that can produce high adsorption efficiency and faster kinetics. Besides, the adsorption of Cu(II) by external magnetic field by MNP ease of synthesis, easy recovery, absence of secondary pollutants, cost-effectiveness, and environmental-friendliness. It can be concluded that MNP promises advanced adsorbent in environmental pollution cleanup. In future works, a surface coating on the magnetic particles needs to be conducted to reduce the particle agglomeration in the sample and enhance the adsorption capacity of Cu(II) ion.

#### Acknowledgments

The authors would like to thank the Department of Physics, Faculty of Science, Universiti Putra Malaysia (UPM), and the Institute of Advanced Technology (ITMA) and for

use of laboratory facilities. The authors also would like to thank the Universiti Putra Malaysia (UPM) and the Ministry of Higher Education Malaysia (MOHE), for the financial support through research grants Nos. (UPM/700-1/2/GPPI/2017/954160), UPM/GP/IPS/958060, UPM/800/GP/2018/9628400 and FRGS (Vot. No. FR-5524942, FR-5540135).

## References

- [1] X.Y. Wu, S.J. Cobbina, G.H. Mao, H. Xu, Z. Zhang, L.Q. Yang, A review of toxicity and mechanisms of individual and mixtures of heavy metals in the environment, *Environ. Sci. Pollut. Res.*, 23 (2016) 8244–8259.
- [2] C. Femina Carolin, P. Senthil Kumar, A. Saravanan, G. Janet Joshiba, Mu. Naushad, Efficient techniques for the removal of toxic heavy metals from aquatic environment: a review, *J. Environ. Chem. Eng.*, 5 (2017) 2782–2799.
- [3] G. Saxena, D. Purchase, S.I. Mulla, G. Dattatraya Saratale, R.N. Bharagava, Phytoremediation of heavy metal-contaminated sites: eco-environmental concerns, field studies, sustainability issues, and future prospects, *Rev. Environ. Contam. Toxicol.*, 249 (2020) 71–131.
- [4] L.-J. Guo, C.-G. Niu, X.-Y. Wang, X.-J. Wen, G.-M. Zeng, DTC-GO as effective adsorbent for the removal of  $\text{Cu}^{2+}$  and  $\text{Cd}^{2+}$  from aqueous solution, *Water Air Soil Pollut.*, 227 (2016) 169, <https://doi.org/10.1007/s11270-016-2865-4>.
- [5] B. Abussaud, H.A. Asmaly, Ihsanullah, T.A. Saleh, V.K. Gupta, Taharlaoui, M. Ali Atieh, Sorption of phenol from waters on activated carbon impregnated with iron oxide, aluminum oxide and titanium oxide, *J. Mol. Liq.*, 213 (2016) 351–359.
- [6] Z.M. Liu, X. Li, P. Zhan, F.P. Hu, X. Ye, Removal of cadmium and copper from water by a magnetic adsorbent of PFM: adsorption performance and micro-structural morphology, *Sep. Purif. Technol.*, 206 (2018) 199–207.
- [7] R. Ahmad, A. Mirza, Inulin-folic acid/bentonite: a novel nanocomposite for confiscation of Cu(II) from synthetic and industrial wastewater, *J. Mol. Liq.*, 241 (2017) 489–499.
- [8] A.A. Najim, A.A. Mohammed, Biosorption of methylene blue from aqueous solution using mixed algae, *Iraqi J. Chem. Petrol. Eng.*, 19 (2018) 1–11, doi: <https://doi.org/10.31699/IJCPE.2018.4.1>.
- [9] D. NguyenThanh, M. Singh, P. Ulbrich, F. Štěpánek, N. Strnadová, As(V) removal from aqueous media using  $\alpha\text{-MnO}_2$  nanorods-impregnated laterite composite adsorbents, *Mater. Res. Bull.*, 47 (2012) 42–50.
- [10] R.S. Azis, M.M. Syazwan, N.M.M. Shahrani, A.N. Hapishah, R. Nazlan, F.M. Idris, I. Ismail, M.M.M. Zulkimi, I.R. Ibrahim, Z. Abbas, N.M. Saiden, Influence of sintering temperature on the structural, electrical and microwave properties of yttrium iron garnet (YIG), *J. Mater. Sci. - Mater. Electron.*, 29 (2018) 8390–8401.
- [11] N.M. Mohd Shahrani, R. Syahidah Azis, M. Hashim, J. Hassan, Z. Azmi, N. Daud, Effect of variation sintering temperature on magnetic permeability and grain sizes of  $\text{Y}_3\text{Fe}_5\text{O}_{12}$  via mechanical alloying technique, *Mater. Sci. Forum*, 846 (2016) 395–402.
- [12] N. Daud, R. Syahidah Azis, M. Hashim, K.A. Matori, J. Hassan, N.M. Saiden, N.M.M. Shahrani, Preparation and characterization of  $\text{Sr}_{1-x}\text{Nd}_x\text{Fe}_{12}\text{O}_{19}$  derived from steel-waste product via mechanical alloying, *Mater. Sci. Forum*, 846 (2016) 403–409.
- [13] R. Syahidah Azis, M. Hashim, N.M. Saiden, N. Daud, N.M.M. Shahrani, Study the iron environments of the steel waste product and its possible potential applications in ferrites, *Adv. Mater. Res.*, 1109 (2015) 295–299.
- [14] K.D. Gong, Q. Hu, L. Yao, M. Li, D.Z. Sun, Q. Shao, B. Qiu, Z.H. Guo, Ultrasonic pretreated sludge derived stable magnetic active carbon for Cr(VI) removal from wastewater, *ACS Sustainable Chem. Eng.*, 6 (2018) 7283–7291.
- [15] R. Saravanan, M.M. Khan, V.K. Gupta, E. Mosquera, F. Gracia, V. Narayanan, A. Stephen, ZnO/Ag/CdO nanocomposite for visible light-induced photocatalytic degradation of industrial textile effluents, *J. Colloid Interface Sci.*, 452 (2015) 126–133.
- [16] R. Awual, Novel nanocomposite materials for efficient and selective mercury ions capturing from wastewater, *Chem. Eng. J.*, 307 (2017) 456–465.
- [17] S. Sulaiman, R.S. Azis, I. Ismail, H.C. Man, N.A.A. Nazri, Adsorption potential of magnetite nanoparticles for copper removal from aqueous solution, *Int. J. Innovative Technol. Explor. Eng.*, 9 (2019) 5424–5429.
- [18] Q. Li, C.W. Kartikowati, S. Horie, T. Ogi, T. Iwaki, K. Okuyama, Correlation between particle size/domain structure and magnetic properties of highly crystalline  $\text{Fe}_3\text{O}_4$  nanoparticles, *Sci. Rep.*, 7 (2017) 1–7, <https://doi.org/10.1038/s41598-017-09897-5>.
- [19] M. Cabeza, I. Feijoo, P. Merino, G. Pena, M.C. Pérez, S. Cruz, P. Rey, Effect of high energy ball milling on the morphology, microstructure and properties of nano-sized TiC particle-reinforced 6005A aluminium alloy matrix composite, *Powder Technol.*, 321 (2017) 31–43.
- [20] R. Nazlan, M. Hashim, I. Ismail, R.S. Azis, J. Hassan, Z. Abbas, F.M. Idris, I.R. Ibrahim, Compositional and frequency dependent-magnetic and microwave characteristics of indium substituted yttrium iron garnet, *J. Mater. Sci. - Mater. Electron.*, 28 (2017) 3029–3041.
- [21] D. Cao, H. Li, L.N. Pan, J.N. Li, X.C. Wang, P.P. Jing, X.H. Cheng, W.J. Wang, J.B. Wang, Q.F. Liu, High saturation magnetization of  $\gamma\text{-Fe}_2\text{O}_3$  nano-particles by a facile one-step synthesis approach, *Sci. Rep.*, 6 (2016) 1–9, <https://doi.org/10.1038/srep32360>.
- [22] A.A. Alqadami, Mu. Naushad, M.A. Abdalla, T.A. Ahamad, Z.A. AlOthman, S.M. Alshehri, A.A. Ghfar, Efficient removal of toxic metal ions from wastewater using a recyclable nanocomposite: a study of adsorption parameters and interaction mechanism, *J. Cleaner Prod.*, 156 (2017) 426–436.
- [23] N.H. de Melo, M.E. de Oliveira Ferreira, E.M. Silva Neto, P.R. Martins, I.C. Ostroski, Evaluation of the adsorption process using activated bone char functionalized with magnetite nanoparticles, *Environ. Nanotechnol. Monit. Manage.*, 10 (2018) 427–434.
- [24] D.D. Do, Adsorption Analysis: Equilibria and Kinetics, Imperial College Press, London, 1998, pp. 1–18.
- [25] P. Klobes, R.G. Munro, Porosity and Specific Surface Area Measurements for Solid Materials, National Institute of Standards and Technology, U.S. Department of Commerce, Gaithersburg, MD, 2006.
- [26] R. Gnanasambandam, A. Proctor, Determination of pectin degree of esterification by diffuse reflectance Fourier-transform infrared spectroscopy, *Food Chem.*, 68 (2000) 327–332.
- [27] S.L. Iconaru, R. Guégan, C.L. Popa, M. Motelica-Heino, C.S. Ciobanu, D. Predoi, Magnetite ( $\text{Fe}_3\text{O}_4$ ) nanoparticles as adsorbents for As and Cu removal, *Appl. Clay Sci.*, 134 (2016) 128–135.
- [28] R. Ahmad, R. Kumar, S. Haseeb, Adsorption of  $\text{Cu}^{2+}$  from aqueous solution onto iron oxide coated eggshell powder: evaluation of equilibrium, isotherms, kinetics, and regeneration capacity, *Arabian J. Chem.*, 5 (2012) 353–359.
- [29] H. Shahbeig, N. Bagheri, S.A. Ghorbanian, A. Hallajisani, S. Poorkarimi, A new adsorption isotherm model of aqueous solutions on granular activated carbon, *World J. Model. Simul.*, 9 (2013) 243–254.
- [30] C.-H. Weng, Y.-C. Wu, Potential low-cost biosorbent for copper removal: pineapple leaf powder, *J. Environ. Eng.*, 138 (2012) 286–292.
- [31] Y.S. Bulut, Z. Tez, Removal of heavy metals from aqueous solution by sawdust adsorption, *J. Environ. Sci.*, 19 (2007) 160–166.
- [32] M. Erdemoğlu, M. Sarıkaya, Effects of heavy metals and oxalate on the zeta potential of magnetite, *J. Colloid Interface Sci.*, 300 (2006) 795–804.
- [33] Y. Liu, L. Chen, Y.Y. Yang, M.D. Li, Y.Y. Li, Y.H. Dong, The efficient removal of Cu(II) from aqueous solutions by  $\text{Fe}_3\text{O}_4$ @hexadecyl trimethoxysilane@chitosan composites, *J. Mol. Liq.*, 219 (2016) 341–349.

- [34] A. Bajpai, M. Sharma, L. Gond, Nanocomposites for Environmental Pollution Remediation, Inamuddin, S. Thomas, R. Kumar Mishra, A.M. Asiri, Eds., Sustainable Polymer Composites and Nanocomposites, Springer Nature, Switzerland, 2019, pp. 1407–1440.
- [35] X.J. Hu, Y. Hu, G.H. Xu, M. Li, Y.T. Zhu, L. Jiang, Y.Z. Tu, X.Q. Zhu, X.C. Xie, A.M. Li, Green synthesis of a magnetic  $\beta$ -cyclodextrin polymer for rapid removal of organic micro-pollutants and heavy metals from dyeing wastewater, *Environ. Res.*, 180 (2020) 108796, <https://doi.org/10.1016/j.envres.2019.108796>.
- [36] S.S. Banerjee, D.-H. Chen, Fast removal of copper ions by gum arabic modified magnetic nano-adsorbent, *J. Hazard. Mater.*, 147 (2007) 792–799.
- [37] M. Farrokhi, M. Naimi-Joubani, A. Dargahi, M. Poursadeghiyan, H.A. Jamali, Investigating activated sludge microbial population efficiency in heavy metals removal from compost leachate, *Polish J. Environ. Stud.*, 27 (2018) 623–627.
- [38] S.S. Bhargav, I. Prabha, Removal of arsenic and copper metals from contaminated water using iron(III) oxide nanoparticle, *Int. J. Chem. Chem. Eng.*, 3 (2013) 2248–9924.
- [39] K.A. Al-Saad, M.A. Amr, D.T. Hadi, R.S. Arar, M.M. Al-Sulaiti, T.A. Abdulmalik, N.M. Alsahmary, S.H. Al-Yahri, Iron oxide nanoparticles: applicability for heavy metal removal from contaminated water, *Arabian J. Nucl. Sci. Appl.*, 45 (2012) 335–346.
- [40] H. Li, D.-L. Xiao, H. He, R. Lin, P.-L. Zuo, Adsorption behavior and adsorption mechanism of Cu(II) ions on amino-functionalized magnetic nanoparticles, *Trans. Nonferrous Met. Soc. China*, 23 (2013) 2657–2665.
- [41] Y.S. Ho, G. McKay, Pseudo-second-order model for sorption processes, *Process Biochem.*, 34 (1999) 451–465.
- [42] N.A.A. Nazri, R.S. Azis, H.C. Man, A.H. Shaari, N.M. Saiden, I. Ismail, Equilibrium studies and dynamic behaviour of cadmium adsorption by magnetite nanoparticles extracted from mill scales waste, *Desal. Water Treat.*, 171 (2019) 115–131.
- [43] M. Jain, M. Yadav, T. Kohout, M. Lahtinen, V.K. Garg, M. Sillanpää, Development of iron oxide/activated carbon nanoparticle composite for the removal of Cr(VI), Cu(II) and Cd(II) ions from aqueous solution, *Water Resour. Ind.*, 20 (2018) 54–74.
- [44] K. Sudha Rani, B. Srinivas, K. Gouru Naidu, K.V. Ramesh, Removal of copper by adsorption on treated laterite, *Mater. Today: Proc.*, 5 (2018) 463–469.
- [45] S. Ben-Ali, I. Jaouali, S. Souissi-Najar, A. Ouederni, Characterization and adsorption capacity of raw pomegranate peel biosorbent for copper removal, *J. Cleaner Prod.*, 142 (2017) 3809–3821.
- [46] Mu. Naushad, S. Vasudevan, G. Sharma, A. Kumar, Z.A. AlOthman, Adsorption kinetics, isotherms, and thermodynamic studies for Hg<sup>2+</sup> adsorption from aqueous medium using alizarin red-S-loaded amberlite IRA-400 resin, *Desal. Water Treat.*, 57 (2016) 18551–18559.